Analysis of Continuously Varying Kinematics for Prosthetic Leg Control Applications

Kyle R. Embry, *Student Member, IEEE,* and Robert D. Gregg, *Senior Member, IEEE*

***Abstract*—Powered prosthetic legs can improve the quality of life for people with transfemoral amputations by providing net positive work at the knee and ankle, reducing the effort required from the wearer, and making more tasks possible. However, the controllers for these devices use finite state machines that limit their use to a small set of pre-defined tasks that require many hours of tuning for each user. In previous work, we demonstrated that a continuous parameterization of joint kinematics over walking speeds and inclines provides more accurate predictions of reference kinematics for control than a finite state machine. However, our previous work did not account for measurement errors in gait phase, walking speed, and ground incline, nor subject-specific differences in reference kinematics, which occur in practice. In this work, we conduct a pilot experiment to characterize the accuracy of speed and incline measurements using sensors onboard our prototype prosthetic leg and simulate phase measurements on ten able-bodied subjects using archived motion capture data. Our analysis shows that given demonstrated accuracy for speed, incline, and phase estimation, a continuous parameterization provides statistically significantly better predictions of knee and ankle kinematics than a comparable finite state machine, but both methods' primary source of predictive error is subject deviation from average kinematics.**

***Index Terms*—Human locomotion, optimization, predictive models, prosthetic limbs, robot control.**

I. Introduction

People with above-knee amputations face many unique challenges to their quality of life. The vast majority use conventional, unpowered prosthetic legs. These devices can vary widely in purpose and complexity [1], [2], but none can provide the net positive work required at the joints for many daily activities [3]–[5]. This forces the user to expend more energy on compensatory behaviors while walking, which can quickly cause fatigue, limit walking range, [6] and cause lower back pain [7]. Limited mobility can also impact social activity, a major component of quality of life [8].

Powered knee and ankle prosthetic legs strive to improve the quality of life of people with transfemoral amputations by using actuators to perform net positive work. There are currently no commercially available powered knee and ankle prostheses, but several research prototypes show promising results [9]–[11]. For example, powered prostheses have enabled more normative gait kinematics while reducing back muscle activation [12] and hip compensations [13], which are both associated with overuse injuries.

Powered devices must employ intelligent control strategies to best leverage their actuation technology to justify their increased weight. One core control challenge is quickly and accurately determining what ambulation mode or task a user wishes to perform, in order to keep up with the user in real time. For many types of controllers, this is accomplished via a high-level task finite state machine (FSM). In an FSM task controller, the range of tasks a user can perform is broken into discrete activities, and custom control parameters are tuned to perform just those activities [14]. Then, classification algorithms are used to determine what available state is closest to the task the user is currently performing, and that set of parameters is selected [15]–[17]. In the case of prosthetic trajectory-following controllers, which enforce predefined kinematic trajectories for the knee and ankle joint (usually based on experimentally recorded average subject trajectories [18]), a high-level FSM task controller is used to switch between task-dependent trajectories [19]. Changing these trajectories to perform new tasks is important for providing normative biomechanical trends like increased ankle work and power at higher speeds, and greater power production in both joints while walking uphill [19]. For all finite state machines, as the number of available states increases, classification accuracy declines, and the time and expertise needed to tune the system to a user increases [14].

There are three main methods to estimate walking speed using sensors onboard a prosthesis: abstraction models, human gait models, and direct integration [20]. Abstraction models use machine learning to infer the relationship between sensor readings and speed, so they require few modeling assumptions and are flexible to sensor placement, but accuracy often depends on the subject unless there is a huge amount of training data [21]. Human gait models use sensor readings as input to simple gait models to predict speed. This technique rarely requires subject-specific training, but the quality deteriorates if model assumptions are not met [22], [23]. Lastly, direct integration integrates the accelerometer measurements in the world frame to determine velocity [24]. This method requires no training or modeling assumptions but is highly sensitive to sensor noise [25], [26]. Almost all walking incline algorithms, on the other hand, rely on taking measurements of the foot angle during midstance. Midstance is usually defined either by simultaneous contact of the heel and forefoot [3], [27] or

This work was supported by the National Institute of Child Health & Human Development of the NIH under Award Number R01HD094772. This work was also supported by NSF Award CMMI-1637704 / 1854898. The content is solely the responsibility of the authors and does not necessarily represent the official views of the NIH or NSF. Robert D. Gregg, IV, Ph.D., holds a Career Award at the Scientific Interface from the Burroughs Wellcome Fund.

[1] K. Embry is with the Department of Mechanical Engineering, University of Texas at Dallas, Richardson, TX 75080, USA and [2] R. Gregg is with the Department of Electrical Engineering and Computer Science; Robotics Institute, University of Michigan, Ann Arbor, MI, 48109 USA. [1]krembry@gmail.com, [2]rgregg@ieee.org

by minima in foot angular velocity [28]–[31]. Foot angle can be measured by accelerometers alone [32] or the fusion of accelerometer and gyroscope signals [28].

Our previous work showed that a continuous parameterization more accurately predicts average human joint kinematics over a range of speeds and inclines than a finite state machine [33] or linear interpolation [34], particularly when trained on a sparse set of data. This continuous kinematic parameterization over walking speeds and inclines could constitute a significant improvement to trajectory-following controllers by allowing for continuous adaptation to the task being performed (no need to round to the nearest available state) and by providing more accurate kinematic predictions for tasks without any training data. However, our previous work with a continuously varying kinematic model (referred to hereafter as the basis model) benefited from several factors that are not present in practical applications: perfect measurements of percent gait, walking speed, and incline, as well as disregarding the differences between subjects that distinguish subject-specific kinematics from across-subject averages. Individual gait patterns are unique [35], [36] and used in many applications from individualized medical diagnostics [36] to prosthetic motion [37]. Recently, researchers have determined how factors such as gender, age, walking speed, and BMI contribute to an individual's gait [38], [39]. These factors could have a significant impact on the performance of a robotic prosthetic leg and must be understood.

In this work, we address all of these factors to determine the effectiveness of the basis model when applied with imperfect measurements of phase and task, and without specific knowledge of the user's kinematics. This study is conducted in two parts. As speed and incline measurements are sensitive to the sensor hardware and algorithms used [20], we first conduct a pilot study to determine the error distribution of these quantities for our low-impedance robotic prosthetic leg [10], used by three able-bodied subjects walking at a variety of speeds and inclines. Second, we use archival motion capture data to train the basis model and evaluate how accurately it predicts the joint kinematics of 10 able-bodied subjects [40]. For each subject, and all 27 speed/incline combinations in this dataset, we use recorded thigh motion to simulate inertial measurement unit (IMU) readings and force plates in the treadmill to simulate ground contact sensors in the prosthesis. Using these simulated sensor inputs to calculate phase, and taking samples from our speed and incline measurement error distributions for each stride, we use the basis model to predict knee and ankle kinematics and compare them to the measured angles for each subject. We analyze how errors in speed, incline, and phase measurement, model fit, and the individual's kinematic differences from average kinematics all contribute to the overall prediction accuracy. Lastly, we use statistical parametric mapping to compare basis model predictions with that of an FSM to determine the potential benefits of the continuously varying task approach over the state-of-art approach for controlling robotic prosthetic legs.

Section II presents a review of preliminaries (e.g., the basis model), the experimental protocol for the collection of task measurement pilot data, a description of the sensors and algorithms used to measure walking speed, incline, and phase, and how the predictive accuracy of the basis model was evaluated. Section III reports the accuracy of our speed, incline, and phase measurements, and how they affect the overall predictive accuracy of the basis model vs. a finite state machine. Section IV discusses how various measurement errors affect predictive accuracy, how the basis model compares to the finite state machine, and limitations of the study. Finally, Section V concludes the paper and identifies future plans.

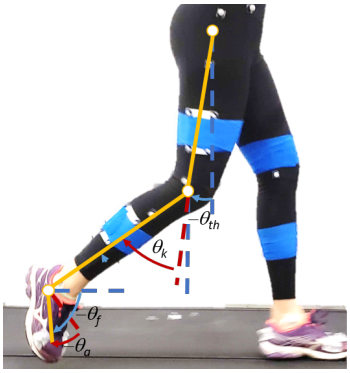

Fig. 1. Definitions of subject coordinates: the angles of the thigh (θ_{th}) and foot (θ_{f}) segments are defined relative to the world frame, and the knee (θ_{k}) and ankle (θ_{a}) angles are defined in the frame of the proximal limb segment. All angles are zero when the subject is standing upright.

II. Methods

A. Preliminaries

This section reviews three prerequisites 1) a publicly available dataset that will be used to train and test our model, 2) the format of the basis model and how to solve for the optimal coefficients given kinematic training data, and 3) the phase variable that will be used to parameterize the basis model.

1) Archival Data: Kinematics Dataset: To compare our predictions of joint kinematics to experimentally recorded kinematics during a variety of walking speeds and inclines, we used archival data from a related study [34]. This data, which is available on IEEE DataPort [40], will be referred to as the kinematics dataset. All 10 able-bodied subjects (5 female) provided written informed consent. The subjects had a mean age of 23 years (SD = 2.8 years), mean height of 170 cm (SD = 8.2 cm), and mean weight of 64 kg (SD = 7.7 kg). A 10-camera Vicon T40 motion capture system (Vicon, Oxford, UK) recorded the subjects' kinematics at 100 Hz while they walked at a steady speed and grade on an instrumented treadmill (Bertec Corp., Columbus, OH) for one minute. For each test, data were collected while the subject walked at a constant speed of 0.8, 1.0, or 1.2 m/s and a constant ground slope ranging from -10° to +10° at 2.5° increments. All subjects walked at every combination of speed and slope, resulting in 27 different tasks with unique identifiers, χ_j with $j = 1, 2, ..., 27$. The order of trials was randomized and subjects took breaks to prevent fatigue. In the dataset, strides were normalized over stride time and interpolated over 150 points in percent gait. Angle definitions are shown in Figure 1.

2) Format and Solution of Basis Model: Embry et al. [34] created a predictive model that represents inter-subject mean gait kinematics as a continuous function of gait phase and task. Gait phase is measured by a phase variable, $\varphi \in \{\mathbb{R}|0 \leq \varphi < 1, \dot{\varphi} > 0\}$, which is a monotonic scalar that increases from 0 to 1 once per stride. Task is represented by $\chi = (\nu, \alpha)$, where ν is the subject's speed linearly mapped from a range of 0.6 m/s to 1.4 m/s to a range of 0 to 1, and α is the ground slope, linearly mapped from -10° to 10° to a range of 0 to 1.

Gait kinematics are modeled as the weighted summation of N basis functions of phase, $b_k(\varphi)$. The weight of each basis function changes for each unique task, as determined by the task functions $c_k(\chi)$. This yields the following separable expression for the joint angle q of the knee or ankle:

$$q(\varphi, \chi) = \sum_{k=1}^{N} b_k(\varphi) c_k(\chi), \tag{1}$$

where the number of basis functions is N, indexed by k.

The basis functions $b_k(\varphi)$ model how joint kinematics progress through the gait cycle. Basis functions are parameterized as finite Fourier series of degree $F = 10$, and these coefficients will be chosen to solve the upcoming optimization problem. The scalar task functions $c_k(\chi)$ model how joint kinematics change in response to speed and slope. Task functions are modeled as 2nd or 3rd degree Bernstein basis polynomials for the terms that operate on speed or slope (see [34, (3)] for details). Together, these basis and task functions create a kinematic model $q(\varphi, \chi)$ that parameterizes how gait cycle, speed, and slope affect the joint kinematics.

The basis model is linear with respect to the parameters of the basis functions, meaning that for a given φ_i and χ_j:

$$\Lambda_{ij} x = \sum_{k=1}^{N} b_k(\varphi_i) c_k(\chi_j), \tag{2}$$

where $x \in \mathbb{R}^{N(1+2F)}$ is a concatenation of the Fourier coefficients from b_k for $k = 1, \ldots, N$. All other terms, which are constants for a given value of φ_i and χ_j, are collected in vector $\Lambda_{ij} \in \mathbb{R}^{1 \times N(1+2F)}$. See [34, (5)] for details. Lastly, in an effort to reduce model complexity and improve predictive performance, automated model order reduction is used to minimize the number of non-zero basis functions. This process is outlined in [34, (7)], and the same reduced set of bases (with coefficients Λ^*_{ij}) will be used in this study.

The kinematic dataset includes thigh, knee, and ankle angular positions at a variety of phases and tasks as described in [40]. We can solve for x such that (1) optimally fits this data. Optimality is defined by this objective function and constraints:

$$\begin{aligned} \underset{x}{\text{minimize}} \quad & \rho + \delta ||\text{vec}(\frac{\partial^3}{\partial \varphi^3} \Lambda^*_{ij} x)||_2, \\ \text{such that} \quad & -\rho \text{SE}(\mathbf{d}_{\varphi_i \chi_j}) \leq \bar{\mathbf{d}}_{\varphi_i \chi_j} - \Lambda^*_{ij} x \leq \rho \text{SE}(\mathbf{d}_{\varphi_i \chi_j}), \\ & R_{\min} < \min_m \Lambda^*_{im} x, \text{ and } R_{\max} > \max_m \Lambda^*_{im} x, \\ & \forall i = 1, ..., 150, \forall m = 1, \ldots, 100, \forall j = 1, \ldots, 27, \end{aligned} \tag{3}$$

where $\bar{\mathbf{d}}_{\varphi_i \chi_j}$ represents the inter-subject mean joint angular position of the knee or ankle recorded at a discrete phase φ_i and task χ_j, and $\text{SE}(\mathbf{d}_{\varphi_i \chi_j})$ represents the standard error of all of the subjects at the given task. This optimization problem seeks to minimize two objectives, ρ and $||\text{vec}(\frac{\partial^3}{\partial \varphi^3} \Lambda^*_{ij} x)||_2$. Scalar ρ acts as a bound on the absolute difference between the inter-subject mean $\bar{\mathbf{d}}_{\varphi_i \chi_j}$ and the value of the basis model evaluated at the same point in phase and task, $\Lambda^*_{ij} x$ (note how ρ appears on both sides of the first inequality constraint). The difference in these two tasks is multiplied by the reciprocal of the inter-subject standard error $\text{SE}(\mathbf{d}_{\varphi_i \chi_j})$. The logic behind this term is that, if all of our subjects had very similar kinematics at a given point (small standard error), it is more important for our mean kinematic surface to match closely at these points. The second objective term, $||\text{vec}(\frac{\partial^3}{\partial \varphi^3} \Lambda^*_{ij} x)||_2$, is a measurement of the jerk in the phase dimension of the basis model. The human body tends to move with jerk-minimized trajectories, and this objective strives to improve biomimicry [41], [42]. The relative weight between our two objectives, fitting the available data and reducing model jerk, is determined by the coefficient δ. Lastly, we also constrain that the model always stays within range of motion bounds $R_{\min}$ and $R_{\max}$. We check this bound at 100 evenly spaced values of speed and grade, indexed by m. This optimization problem can easily be solved with a convex optimization solver like [43], and has a guaranteed globally optimal solution.

3) Phase Variable Definition: A phase variable is a mechanical signal which grows monotonically with the gait cycle, and can be used to estimate gait cycle percentage in real-time applications for prostheses [44] or biped robots [45]. A phase variable is preferable to normalized stride time because it provides a more robust parameterization of kinematics in the presence of perturbations [46]. The phase variable used in this study is based on the fact that the phase portrait of thigh angle $\theta_{\text{th}}(t)$ and the shifted thigh angle integral $\Phi(t) = \int_0^t (\theta_{\text{th}}(\tau) - x_0) d\tau$ form an ellipse over the course of one stride period [19], [47]. The phase variable $\varphi_{\text{th}}(t)$ is defined as the polar angle of this phase portrait:

$$\begin{aligned} \varphi_{\text{th}}(t) &= \left(\text{atan2}(k\Phi(t), \theta_{\text{th}}(t) - x_0) + \pi\right)/2\pi, \\ k &= \frac{|\theta^{\max}_{\text{th}} - \theta^{\min}_{\text{th}}|}{|\Phi^{\max} - \Phi^{\min}|}, \qquad x_0 = \frac{1}{2} \int_0^T \theta_{\text{th}}(t) dt, \end{aligned} \tag{4}$$

where T is the time period of the stride and the scaling parameter k changes the phase portrait into approximately a circle instead of an ellipse, and the shifting parameter x_0 centers the phase portrait at the origin. These scale and shift parameters are important for maintaining the monotonicity and approximate linearity of the phase variable during steady state walking. For real-time application, at every heel strike t_{HS}, we define that $\Phi(t_{\text{HS}}) = 0$ and $\varphi_{\text{th}}(t_{\text{HS}}) = 0$ and update $\theta^{\min}_{\text{th}}, \theta^{\max}_{\text{th}}, \Phi^{\min}, \Phi^{\max}$, and x_0 based on their values in the previous stride. This ensures that these constant parameters adapt to changing conditions with the subject. As discussed in [47], changing these parameters too quickly can have negative effects on walking stability in practice. To mitigate this issue for real-time phase calculation, we saturated each of these parameters to ± 1 unit change from their previous value each stride. For offline (non-causal) calculation, these parameters are determined by recording the true value of these parameters

over an entire gait cycle before calculating the phase variable. This offline approach is referred to as the ideal phase variable. The ideal phase variable is used to parameterize the training data because it has the same average trajectory as the real-time phase variable, as will be shown in subsection III-A.

B. Kinematic Surface Parameterized by Thigh Phase Variable

The results of [34] used percent gait, Γ, to parameterize the evolution of joint trajectories during a gait cycle, but real-time phase variables such as (4) are used in practice [19]. While the phase variable (4) tends to increase monotonically through the gait cycle, the progression is not linear with time. In this work, we explicitly synchronize our encoded joint progression with the expected evolution of our phase variable under various conditions. To do so, we determined the time-evolution of the phase variable for each walking task, and parameterize the joint kinematics by phase instead of percent gait before refitting the model to the kinematic data using (3). We calculated a phase variable based on the across-subject average thigh trajectory as described in (4), using the ideal offline values for k and x_0. If the phase variable for a task was not strictly monotonic, strict monotonicity was enforced using a rate-limiting filter that enforced a minimum slope of +0.5 $\mathrm{d}\varphi_{\mathrm{th}}/\mathrm{d}\Gamma$. The phase variable almost always exceeded this rate, but the filter was critical for enabling reparameterization in a few examples where strict monotonicity was briefly violated. After phase variable calculation, the knee and ankle trajectories were reinterpolated to 150 points evenly-spaced in phase instead of time, and these new trajectories were used to solve the optimization problem (3) again. This reinterpolation preserved the amplitude of the knee and ankle trajectories, but phase shifts them based on the nonlinear evolution of the phase variable. See Figure 2 for an example of how this reparameterization affected average trajectories. Note that the uphill phase trajectories are more linear because the thigh phase portrait is more circular [48], which more closely matches the assumptions in the phase variable derivation [46].

C. Task Measurement Pilot Experiment

Data were collected to determine the accuracy of walking speed and incline estimation using only sensors onboard our prototype robotic knee-ankle prosthesis [10]. The experimental protocol was approved by the Institutional Review Board at the University of Texas at Dallas. Informed consent was provided by three able-bodied subjects with mean age 30 years (SD = 7.9 years), mean height 181 cm (SD = 7 cm), and mean weight 84.6 kg (SD = 11.9 kg). Subjects were equipped with a bypass adapter to wear the robotic prosthetic leg. Subjects were given time to acclimate to walking with the prosthesis before data collection. During each trial, the subjects walked on a commercial treadmill at a constant speed of 0.63, 0.85, or 1.07 m/s and a constant ground slope of -1.9, 0.3, or 5.5 deg. Motion capture markers on the prosthetic foot were used to externally verify the walking speed during the stance period, and markers on the treadmill frame were used to verify incline. Subjects walked for one minute at every combination of these speeds and inclines, for a total of nine trials.

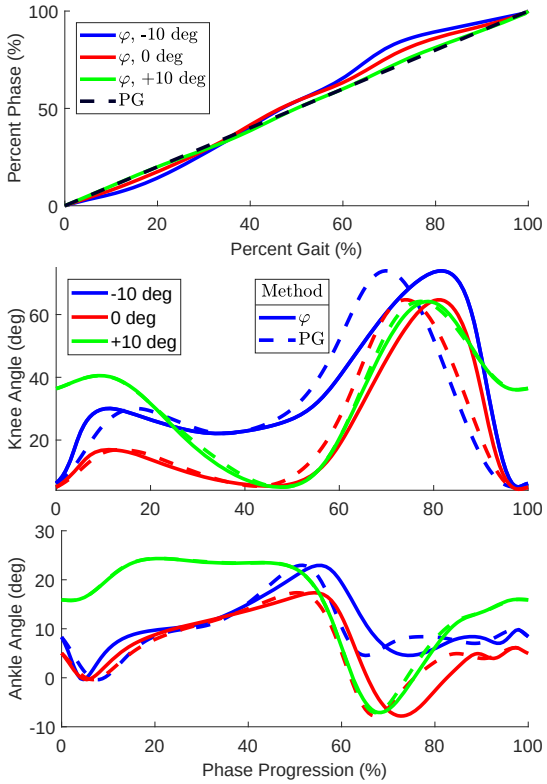

Fig. 2. Parameterization by phase variable (φ, solid lines) vs. percent gait (PG, dashed lines) for three example tasks: walking at 1 m/s on a -10° (blue), 0° (red), and +10° (green) incline. Trajectories represent across-subject averages. The phase variable plot (top) shows both φ and PG scaled from 0 to 100% on the vertical axis.

During the task measurement pilot experiment, the prototype leg was controlled using the impedance-based controller described in [10]. The impedance parameters were changed before each trial to ensure the subject could walk safely at that speed and incline. The trial order was randomized and frequent breaks were offered to mitigate the effects of fatigue. During every trial, data were recorded using IMUs built into the foot and thigh segments of the leg, as well as the joint encoders and load cells in the ankle. Our prototype was equipped with 3DM-CX5-25 and 3DM-GX4-25 IMUs, (LORD Microstrain, VT, USA) on the thigh and instep, respectively. The instep IMU was connected directly to the carbon fiber prosthetic foot, beneath the cosmesis, to ensure rigid alignment with the foot segment. The knee and ankle encoders were optical quadrature encoders, E5 and EC35 (US Digital, WA, USA), respectively, and provided high-precision measurements of joint angles. Lastly, the ankle load cell was a M3564F 6-axis load cell (Sunrise Instruments, Nanning, China) and was used exclusively for stance detection in this experiment. Estimates of the subjects' walking speed and incline were made offline based on sensor recordings.

D. Task Variable Measurement

In the task measurement pilot experiment, average speed estimates were made once per stride and filtered with a moving average filter. The speed estimates are based on a double-pendulum model of human walking, and utilized measurements of the thigh angle (from a thigh-mounted IMU),

knee angle (from a joint encoder), and measurements of the subject's thigh and tibia lengths (measured before the experiment), in a manner similar to [49]. This model assumed that the distance travelled by the subject during one stride is equal to the summation of the foot's displacement with respect to the hip during stance and swing. The foot's position with respect to the hip joint center p_{fh} is

$$p_{\text{fh}}(t) = L_{\text{th}} \begin{bmatrix} \cos(\theta_{\text{th}}(t)) \\ \sin(\theta_{\text{th}}(t)) \end{bmatrix} + L_{\text{ti}} \begin{bmatrix} \cos(\theta_{\text{th}}(t) + \theta_{\text{k}}(t)) \\ \sin(\theta_{\text{th}}(t) + \theta_{\text{k}}(t)) \end{bmatrix}, \quad (5)$$

where L_{th} and L_{ti} are the lengths of the subject's thigh and tibia. The displacement during stance and swing are measured at every ipsilateral heel strike (HS) or toe-off (TO) event:

$$\begin{aligned} &\text{if } t = t_{\text{TO}}, \qquad d_{\text{stance}} = \|p_{\text{fh}}(t_{\text{TO}}) - p_{\text{fh}}(t_{\text{HS}}^-)\|_2, \\ &\text{if } t = t_{\text{HS}}, \qquad d_{\text{swing}} = \|p_{\text{fh}}(t_{\text{HS}}) - p_{\text{fh}}(t_{\text{TO}}^-)\|_2, \end{aligned} \quad (6)$$

where t_{TO}^- and t_{HS}^- are the times of the previous TO or HS event, respectively. Then at every HS event the average speed of the stride can be updated:

$$\begin{aligned} &\text{if } t = t_{\text{HS}}, \qquad \nu(t) = (d_{\text{stance}} + d_{\text{swing}})/(t_{\text{HS}} - t_{\text{HS}}^-), \\ &\text{otherwise}, \qquad\qquad\qquad\quad \nu(t) = \nu(t-1). \end{aligned} \quad (7)$$

The walking speed was assumed constant until updated at the next HS event. A moving average filter based on the current and two previous strides reduced noise in the speed estimation.

Incline estimates were updated once per stride, based on measurements of foot angle during midstance, similar to [31]. The stance foot was determined to be in midstance if the foot gyroscope signal had an absolute value less than 0.4 rad/s. After TO, the mean of all foot angles that occurred during midstance was used to estimate the incline of that stride.

E. Simulation Overview

To study the use of the basis model in a trajectory-following controller, we made predictions of knee and ankle kinematics for all 10 able-bodied subjects and all 27 speed/incline combinations recorded in the kinematics dataset [40]. Each trial is 60 seconds long and recorded at 100 Hz, giving us approximately 1.6 million timesteps to evaluate. The accuracy of the basis model was determined by measuring the difference between the basis model's kinematic predictions and the recorded kinematics at each timestep.

The basis model requires three inputs to estimate joint kinematics: phase, speed, and incline. As the archival kinematic dataset does not include IMU data, we used motion capture thigh angle measurements and treadmill force plate signals to calculate the real-time phase variable (4) at each timestep in the dataset. While not equivalent measurements, motion capture is often used as ground truth for kinematics, and the 3DM-CX5-25 IMU has a rated angular position accuracy of 0.25 deg RMS [50]. We believe this substitution is acceptable for the goals of this study because even less accurate IMU sensors have nearly 99.58% correlation with motion capture thigh angle measurements [51]. Speed and incline measurements, however, are sensitive to the exact sensors and algorithms used [20], so there are no appropriate substitutes in the archival kinematic dataset. To simulate speed and incline measurement error, we randomly sampled measurement errors once per stride from the error distributions determined in the task measurement pilot experiment (subsection II-C). With all three inputs determined, we used the basis model to predict joint kinematics at every timestep of the archival dataset.

Lastly, we also used our phase, speed, and incline estimates to calculate joint kinematics using a finite state machine. This FSM rounded the incline measurement (with simulated error) to the nearest of these three inclines: [-7.5, 0, 7.5] degrees, and assumed the walking speed was always 1.0 m/s. These states were selected due to their centrality within the tasks that will be tested: the finite state machine will never have to round incline more than 2.5 degrees, or speed by more than 0.2 m/s. Once a state is selected, kinematics are calculated using the real-time phase variable input to an 8th order Fourier fit of the average kinematics of the corresponding state.

F. Analysis Overview

Beyond determining the overall predictive accuracy, we determined what factors play a dominant role in causing the overall predictive error. We identified five error factors that affect the overall predictive accuracy: 1) speed measurement error, 2) incline measurement error, 3) phase measurement error, 4) model fitting errors, and 5) subject deviations from the across-subject average kinematics. The first three factors are related to errors in the input of the basis model, which naturally cause errors in the output. However, these effects are highly nonlinear, e.g, using +1 deg as the input when the true incline is 0 deg changes the kinematic prediction differently than using +10 deg when the true incline is +9 deg. To normalize the kinematic effect of input errors, we calculated several versions of predicted kinematics, each with only one factor in error. For example, to determine the kinematic effect of speed measurement error, we calculated the basis model's output with speed measurement errors but perfect incline and phase measurement. We then find the difference between these predictions and model predictions with no input errors and call this difference the kinematic speed error. Analogous steps are used to determine the incline and phase kinematic error.

Model fitting error exists because the basis model is a low-rank predictive model, not an interpolant. This means that it does not match the training data it is given exactly, but makes compromises in fitting to encourage smoothness in output and decrease the complexity of the fitting terms. As shown in [34], this approach provides statistically significantly better prediction of untrained tasks than a linear interpolant. Model fitting error is therefore defined as the difference between the value of the basis model with no input errors, and the value of the average subject kinematics (the training data for the basis model) at the exact same point in speed, incline, and phase. This quantity was calculated for every timestep in the experiment. To determine the average kinematics at arbitrary points in phase, the average kinematic trajectories were fit with an 8th order Fourier function for every task.

Lastly, subject deviations from the average kinematics have two causes: the differences between the mean kinematics of a given subject compared to the across-subject average, and the

stride-to-stride variations that cause a subject's kinematics to vary from their mean. To measure the combined effect of these two causes, we define "individuality" as the difference between the kinematics of an individual at a given timestep, and the kinematics of the average subject at the same value of speed, incline, and phase (again, using an 8th order Fourier function). The basis model was fit to across-subject average kinematics, so an individual's deviation will result in a predictive error.

To determine each factor's relationship with the overall fitting error, we constructed a linear mixed-effects model. Linear mixed-effect models represent a response variable as a linear function of several independent variables, which can be fixed or random [52]. In our case, the overall predictive error was the response variable, kinematic error factors were modeled as fixed variables, and an intercept unique to each subject was modeled as a random variable. This analysis returned a coefficient describing the linear relationship between the independent variables and response variables (for an optimal model that considers the effect of all independent variables) as well as confidence intervals for that coefficient and a p-value that reports the likelihood that this coefficient is different from zero. Overall, this gave us a better understanding of how the five error factors contribute to the overall error.

To compare the predictive accuracy of the basis method to a finite state machine, we used statistical parametric mapping, or SPM. SPM incorporates random field theory to compare groups of time-trajectories while explicitly accounting for temporal correlation [53]. In our case, we used SPM to perform a paired, two-tailed t-test on the absolute predictive error presented by the basis method and an FSM. The result indicates which method has statistically significantly lower predictive error over different regions of the gait cycle. This analysis was performed for all subjects and tasks simultaneously, allowing us to obtain a very high-level understanding of how each method is performing over a gait cycle.

III. Results

A. Phase Variable Reparameterization and Accuracy

The across-subject average joint trajectories (used in the FSM or to train the basis model) were first reparameterized by the expected trajectory of a phase variable to maintain synchronization between the subject and kinematic predictions, as discussed in subsection II-B. In practice, errors in real-time phase parameter estimation cause the phase variable trajectory to vary from the ideal phase variable in curvature or final value. To determine how much these parameter estimates affect real-time implementation, we calculated the phase variable for every subject, trial, and timestep in the kinematics dataset using both real-time parameter estimation, and non-causal, ideal identification of parameters. The kinematics dataset contains approximately 4.5 hours of motion capture data at 100 Hz, or about 1.6 million timesteps. The difference in phase variable was defined as phase variable error, shown in Figure 3. Note that to improve the readability of this histogram, only the inner 99% percent of phase errors are plotted. The remaining 1% lie between the bounds shown and the full range of possible phase errors, [-1,1).

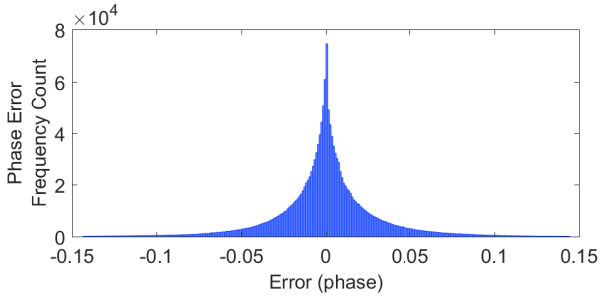

Fig. 3. Histogram showing the inner 99% of phase errors in the simulation.

B. Task Variable Accuracy

Speed estimation during the task measurement pilot experiment was based on a two-link model of human walking, using measurements of segment lengths and joint angles to estimate a stride length, which was divided by stride time to determine average speed. For every stride, we determined speed estimation accuracy by subtracting the speed estimate from the true speed measured with motion capture (positive errors are over-estimates, negative errors are under-estimates). The three subjects individually had mean speed errors of 0.007, 0.018, and -0.033 m/s. The three walking speeds tested (0.63, 0.85, 1.07 m/s) had mean speed errors of 0.030, 0.025, and -0.052 m/s, respectively. Because these subject-specific and speed-specific means are small and the overall error is centered at zero, every trial in the simulation sampled errors from a normal distribution with μ = 0 deg, SD = 0.066. After concatenating the set of error values for all subjects, inclines, and speeds, Figure 4 (top) shows a histogram and the best-fit normal distribution that approximates the overall error for all 749 strides with speed estimations.

Incline estimation during the task measurement pilot experiment was based on measuring of the foot angle during midstance. However, it was noted after the experiment that some of the trials encountered foot angular rotation rates over 8.4 radians/second, which caused saturation of our IMU's gyroscope. This did not impact midstance detection which is based on very small gyroscope measurements. However, the complementary filter running onboard the IMU cannot overcome the saturated gyroscope signal, resulting in unreliable foot orientation measurements. Future work can overcome this limitation by using a different version of the LORD Microstrain IMU 3DM-CX5-25, which has a 15.7 rad/s gyroscope. Due to this implementation issue, only trials where the foot gyroscope saturated less than 10% of the time are considered for accuracy analysis. Specifically, all of the 0.85 and 1.07 m/s trials exceeded the gyroscope's limit, as well as the 0.63 m/s uphill trial of one subject, leaving eight trials left which can be analyzed for incline accuracy. For all of the 180 remaining strides, we determined accuracy by subtracting the incline estimate from the true incline measured with motion capture (positive errors are over-estimates, negative errors are under-estimates). The three subjects individually had mean errors of 0.006, -0.370, and 0.290 deg. The three inclines tested (-1.9, 0.3, 5.5 deg) had mean errors of 0.014, -0.086, and 0.100 deg, respectively. Because these subject-specific and incline-specific means are small and the overall error is centered at

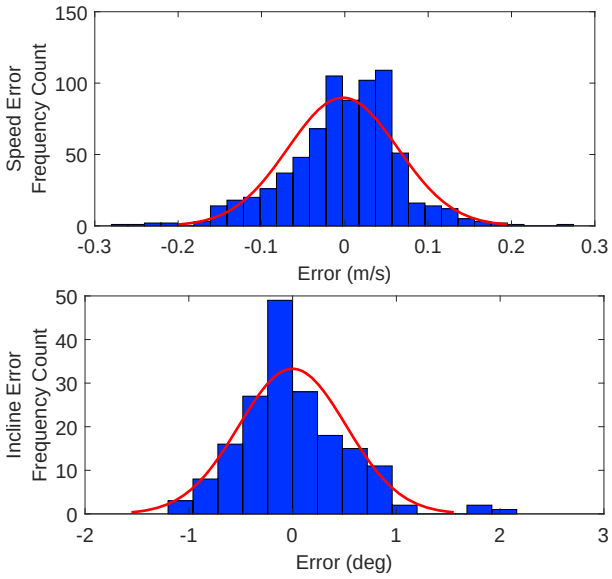

Fig. 4. Histograms and normal distribution approximation of all errors encountered in the task measurement pilot experiment. The frequency count of the incline graph (bottom) is lower than the speed graph (top) due to the number of trials eliminated for saturating the foot IMU gyroscope.

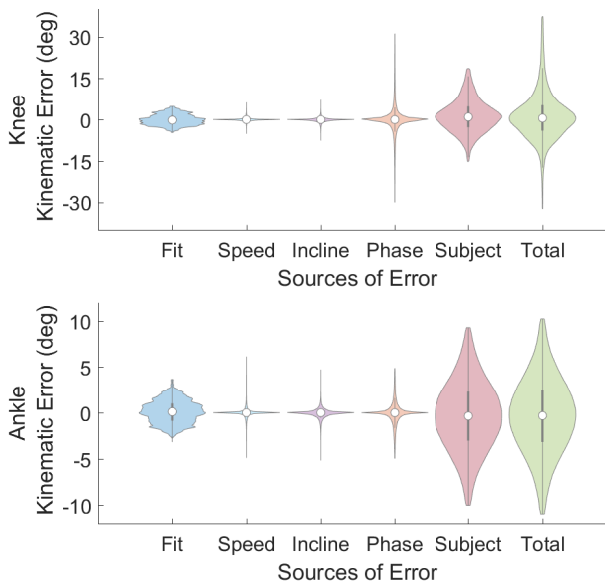

Fig. 5. Violin plots comparing total error to the expected error due to all five major error factors. For visibility, only the inner 97% of errors are plotted for Phase, Subject, and Total. Subject is the largest error source by far.

zero, every trial in the simulation sampled errors from a normal distribution with μ = 0 deg, SD = 0.52. Figure 4 (bottom) shows a histogram and the best-fit normal distribution that approximates the overall error.

C. Kinematic Error Factors

As previously stated, five major factors contribute to error in kinematic predictions: measurement error in the three required inputs (speed, incline, and phase), errors in fitting a model to average subject data, and subject-specific differences from the average subject. Figure 5 shows a violin plot of the errors from each source, compared to the total error. These violin plots show the kernel density estimate of each factor; for every point on the y-axis, the width of the plot show what percentage of data exhibits that much error (similar to a probability density function) [54]. These factors exhibit different results in terms of probability distribution and maximum errors.

D. Predictive Kinematics Accuracy

Table I shows the relationship between each of our kinematic error factors and the overall error for all subjects and tasks. The (Intercept) field shows the value of the constant error offset, which was small for both joints. The estimates column shows the regression coefficient for each factor. These regression coefficients are the slope of the linear relationship between error factors and kinematic prediction error. Most of our error factors have values around 0.95, indicating that when any error factor changes by one degree, the overall error changes by about 0.95 deg. The positive slope indicates that the changes are proportionate. The p-values shown in the table indicate that the regression coefficients are significant, and the 95% confidence interval shows the range of possible coefficient values. Random effects report standard deviation and accompanying 95% confidence interval instead. The (Intercept):Subject field shows the SD of the random intercepts fitted to each subject, which is small for both joints. The Residual SD field shows the SD of the residuals after accounting for fixed and random effects. For reference, the total knee kinematic error had a SD of 12.33, while the total ankle kinematic error had a SD of 4.68. The residual SD of 3.351 and 0.340 show that the mixed linear model is accounting for the majority of the experimental variance.

E. Statistical Parametric Mapping, Basis vs. FSM

Figure 6 shows the result of the SPM analysis comparing the basis method accuracy with that of an FSM, for all subjects and tasks. The black line indicates the t-value for a paired, two-tailed SPM t-test. When the t-value is greater than the critical value z^* (blue line), the basis method has statistically significantly less error than the FSM method, and the $y = 0$ line is highlighted blue. Conversely, when the t-value is less than $-z^*$ (red line), the FSM method has significantly less error, and the $y = 0$ line is highlighted red. If there is no highlight, neither method is statistically significant.

IV. Discussion

A. Kinematic Factors that Affect Model Predictions

One interesting finding from this work is that our linear mixed-effect model was able to explain most of the total kinematic error variance using coefficients close to one for all error factors. This would imply that for future work, we may be able to estimate the total error by simply summing the average effect of each factor. If errors become significantly larger, the nonlinear effects of the model may become more dominant and this approximation would no longer be appropriate.

Our reported speed estimation residual standard deviation (SD=0.066, also known RMSE) was nearly identical to the errors reported in the source of our algorithm (0.06 m/s

TABLE I
MIXED LINEAR EFFECT RESULTS

	Knee $R^2 = 0.9261$			**Ankle $R^2 = 0.9947$**		
Fixed Effects	**estimate**	**95% CI**	***p***	**estimate**	**95% CI**	***p***
(Intercept)	0.444	0.349 / 0.540	<<0.001	-0.007	-0.009 / -0.005	<<0.001
speed	0.923	0.913 / 0.932	<<0.001	0.949	0.948 / 0.950	<<0.001
incline	0.983	0.977 / 0.990	<<0.001	1.003	1.001 / 1.004	<<0.001
phase	0.952	0.952 / 0.953	<<0.001	0.987	0.987 / 0.987	<<0.001
individuality	0.967	0.966 / 0.967	<<0.001	1.000	1.000 / 1.000	<<0.001
model fit	1.059	1.056 / 1.061	<<0.001	1.000	1.000 / 1.001	<<0.001
Random Effects	**SD**	**95% CI**		**SD**	**95% CI**	
(Intercept):Subject	0.153	0.099 / 0.237		0.003	0.002 / 0.005	
Residual SD	3.351	3.348 / 3.355		0.340	0.340 / 0.341	

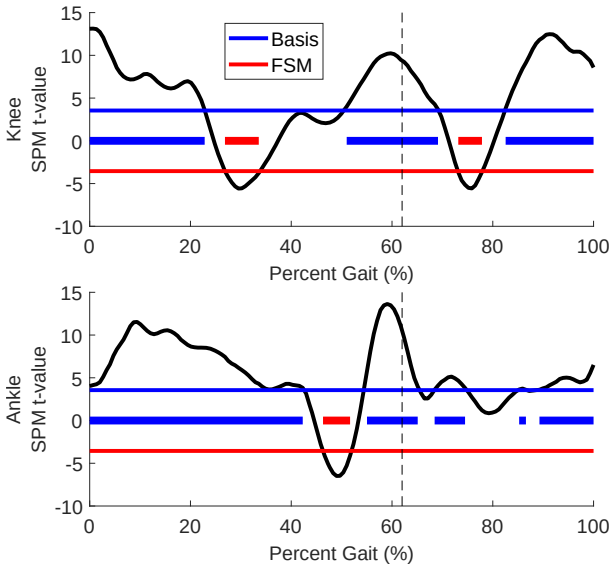

Fig. 6. The SPM t-value indicating which method creates statistically significantly less error for the gait cycle of the knee (top) or ankle (bottom). The colored bars across $y = 0$ indicate which method has statistically lower error in that region of the gait cycle, as determined by an SPM two-tailed t-test. 62% gait is highlighted to show the expected end of the stance period.

RMSE) [49]. This places our measurement on par or better than many alternative methods [55]–[57]. Our incline estimation algorithm produced an RMSE error of 0.52 deg, and a maximum error of 2.04 degrees. This places it among similar methods like [55], which reports 0.64 - 1.00 deg RMSE for incline detection (depending on the subject, see [55, Table I]) and other IMU-based methods [3], [32]. Our errors are somewhat higher than those presented by [30], which uses an interesting IMU / EMG fusion algorithm to determine ground slope. Our kinematic error analysis (Figure 5) indicates that these state-of-the-art speed and incline measurements are sufficiently accurate to not play a dominant role in creating error in kinematic predictions.

The model fit kinematic factor has a qualitatively different distribution than other factors due to the choice of maximum absolute error between the model and data as the objective function in the optimization. Its resulting error distribution shows that the model fit has the smallest maximum error of any factor, but the error is more uniformly distributed throughout the total range. Model fitting error is not due to random changes in input measurement but is the result of the compromises necessary to fit many different tasks with a low-rank model. Large errors in model fitting would indicate consistently large kinematic errors at some point in the phase/task space rather than random occurrences.

This study provides a unique analysis of phase variable accuracy by comparing online and offline phase algorithms. We showed that while phase input errors are a small portion of the overall predictive error, there exist infrequent measurements that cause large kinematic errors. While this analysis has not been performed previously, the algorithm used is very similar to previous work [47]. These results could likely be improved by filtering techniques that determine the certainty of each phase parameter while estimating their values.

Finally, subject individuality played the most critical role in determining the overall predictive accuracy. This finding is congruent with previous work, as the basis method (and the comparable finite state machine used in this study) are designed to predict average kinematics, with no accommodation for stride-to-stride variance or the specific subject using the prosthesis. Previous work has shown that providing average-subject kinematics is still an effective method for improving amputee gait [13], [19], and that it is possible, and practical, to tune the kinematic trajectories of individual tasks to better match a subject in a clinical setting [18]. Concurrently, recent work has shown that the continuous format of the basis model can be leveraged to improve the tuning of all tasks, given one tuned task [58]. This work is particularly promising, as it demonstrated that for most subjects it provides a reduction in mean and max individualization error for all joints based on a very simple tuning procedure. This kinematic tuning method could enable us to use clinician feedback to better determine the mean kinematic trajectory preferences of an individual within one visit to their clinician. Leveraging that information, we can create new kinematic models that are custom-made to the individual, reducing the individuality kinematic error. It should be noted that this subject-specific tuning can be applied to an FSM with predefined kinematics also, but improving both methods in this fashion would still leave the basis method at a relative advantage due to its superior modeling of the effects of task on human gait.

To demonstrate this idea, we conducted a secondary analysis for predicting one subject's kinematics with a basis model trained using only data from the same subject. We found that the subject individuality term (which now only represents stride-to-stride variance from the subject's mean kinematics) was about 40% smaller than the individuality error found using

the across-subject average model, in terms of mean absolute error. This reduced the overall error by about 20%. These results imply that subject-specific tuning could be capable of reducing the predictive error of the basis method by a significant amount. Future work on tuning propagation may prove critical in reducing the largest remaining hurdle to accurate kinematic predictions for individuals.

B. Comparison to Finite State Machine

The results of Figure 6 show that the basis model provides a relatively small but statistically significant improvement over the predictions made by an FSM. There are several reasons for this difference. Both of these algorithms share the phase and subject individuality kinematic error factors, which are the largest sources of the overall error. If these two factors can be reduced, by tuning and improving the phase variable calculation and employing subject-specific tuning techniques [18], [58], the relative advantage of the basis method would be more significant. Lastly, three of the test tasks in this study matched the available tasks in the state machine exactly. For those three tests, the FSM would have effectively zero speed kinematic error, incline kinematic error, or kinematic model error. In more practical applications, users will rarely choose to walk at the exact speed and inclination that the prosthetic controller was designed for.

C. Limitations and Future Work

While we did analyze what kinematic errors result from using a real-time measurable phase variable instead of an ideal phase variable, we did not study how a phase variable calculated from a motion capture thigh angle varies from one calculated on a wearable IMU. While similar, these orientation measurements are not identical and will suffer from different failure modes. Another limitation is that the speeds and inclines that were tested for accuracy in the task measurement pilot experiment do not exactly match the speeds and inclines analyzed in simulation. Since the error of both measurements did not vary greatly with respect to speed or incline, we believe this did not have a great impact on the conclusion. The issues we encountered with gyroscope saturation limit the thoroughness of our incline estimation error at all speeds. However, we have verified that there are commercially available IMUs with sufficient gyroscopic range to measure all activities discussed in this paper. Lastly, the results of this paper only indicate that the basis method generally provides statistically significantly better predictions of kinematics than an FSM. Further clinical testing will be required to determine clinical significance.

V. Conclusion

This study reported speed measurements with less than 0.06 m/s RMSE and incline measurements with less than 0.52 degs RMSE, using only sensors onboard a prosthetic leg. This accuracy is very comparable to other state-of-the-art IMU approaches. Using these task measurements, we demonstrated that the basis method provides more accurate predictions of kinematics for individual subjects than a finite state machine for most of the gait cycle. The primary factors reducing predictive accuracy are speed measurement error, incline measurement error, phase measurement error, model fit, and subject individuality. A linear mixed-effects model proved that subject individuality was by far the largest source of predictive error, meaning that future work should focus on individualizing kinematics for each user. Promising work in this field has already begun, including visual techniques for in-clinic kinematic tuning of a prosthesis [18], and using the basis model to predict variable-activity kinematics for individual subjects based on very little subject-specific data [58].

There are several avenues for continued work. We aim to model other ambulation modes using the methods described in this study, create transitional task variables to aid in switching between gait controllers, and utilize expert clinical tuning and task propagation to quickly improve the gait performance of users across all tasks. All of these systems will be tested in real-time controllers on our robotic leg prototype.

Acknowledgment

The authors thank Corey Powell of the University of Michigan CSCAR team for statistical consultation, Toby Elery for help with the powered prosthetic leg experiments, and Lizbeth Zamora for help with processing experimental data.

References

[1] J. W. Michael and J. H. Bowker, *Atlas of amputations and limb deficiencies: surgical, prosthetic, and rehabilitation principles*. American Academy of Orthopaedic Surgeons, 2004.

[2] K. R. Kaufman, J. A. Levine, R. Brey, B. Iverson, S. McCrady, D. Padgett, and M. J. Joyner, "Gait and balance of transfemoral amputees using passive mechanical and microprocessor-controlled prosthetic knees," *Gait & posture*, vol. 26, no. 4, pp. 489–493, 2007.

[3] F. Sup, H. A. Varol, and M. Goldfarb, "Upslope walking with a powered knee and ankle prosthesis: initial results with an amputee subject," *IEEE Trans. Neural Syst. Rehabil. Eng.*, vol. 19, no. 1, pp. 71–78, 2011.

[4] B. E. Lawson, H. A. Varol, A. Huff, E. Erdemir, and M. Goldfarb, "Control of stair ascent and descent with a powered transfemoral prosthesis," *IEEE Trans. Neural Syst. Rehabil. Eng.*, vol. 21, no. 3, pp. 466–473, 2012.

[5] A. H. Shultz, B. E. Lawson, and M. Goldfarb, "Running with a powered knee and ankle prosthesis," *IEEE Trans. Neural Syst. Rehabil. Eng.*, vol. 23, no. 3, pp. 403–412, 2015.

[6] I. M. Starholm, P. Mirtaheri, N. Kapetanovic, T. Versto, G. Skyttemyr, F. T. Westby, and T. Gjovaag, "Energy expenditure of transfemoral amputees during floor and treadmill walking with different speeds," *Prosthet Orthot Int*, vol. 40, no. 3, pp. 336–342, 2016.

[7] D. M. Ehde, D. G. Smith, J. M. Czerniecki, K. M. Campbell, D. M. Malchow, and L. R. Robinson, "Back pain as a secondary disability in persons with lower limb amputations," *Arch Phys Med Rehabil*, vol. 82, no. 6, pp. 731–734, 2001.

[8] W. C. Miller, A. B. Deathe, M. Speechley, and J. Koval, "The influence of falling, fear of falling, and balance confidence on prosthetic mobility and social activity among individuals with a lower extremity amputation," *Arch Phys Med Rehabil*, vol. 82, no. 9, pp. 1238–1244, 2001.

[9] F. Sup, H. A. Varol, J. Mitchell, T. J. Withrow, and M. Goldfarb, "Preliminary evaluations of a self-contained anthropomorphic transfemoral prosthesis," *IEEE/ASME Trans. Mechatronics*, vol. 14, no. 6, pp. 667–676, 2009.

[10] T. Elery, S. Rezazadeh, C. Nesler, and R. D. Gregg, "Design and validation of a powered knee-ankle prosthesis with high-torque, low-impedance actuators," *IEEE Trans. Robot.*, 2020.

[11] A. F. Azocar, L. M. Mooney, L. J. Hargrove, and E. J. Rouse, "Design and characterization of an open-source robotic leg prosthesis," in *IEEE Int Conf Biomed Robot Biomechatron*, 2018, pp. 111–118.

[12] C. Jayaraman *et al.*, "Impact of powered knee-ankle prosthesis on low back muscle mechanics in transfemoral amputees: A case series," *Frontiers in neuroscience*, vol. 12, p. 134, 2018.

[13] T. Elery, S. Rezazadeh, E. Reznick, L. Gray, and R. D. Gregg, "Effects of a powered knee-ankle prosthesis on amputee hip compensations: A case series," *IEEE Trans. Neural Syst. Rehabil. Eng.*, 2020.

[14] A. M. Simon, K. A. Ingraham, N. P. Fey, S. B. Finucane, R. D. Lipschutz, A. J. Young, and L. J. Hargrove, "Configuring a powered knee and ankle prosthesis for transfemoral amputees within five specific ambulation modes," *PloS one*, vol. 9, no. 6, p. e99387, 2014.

[15] A. J. Young, A. M. Simon, N. P. Fey, and L. J. Hargrove, "Intent recognition in a powered lower limb prosthesis using time history information," *Ann. Biomed. Eng.*, vol. 42, no. 3, pp. 631–641, 2014.

[16] R. Jiménez-Fabián and O. Verlinden, "Review of control algorithms for robotic ankle systems in lower-limb orthoses, prostheses, and exoskeletons," *Med. Eng. Phys.*, vol. 34, no. 4, pp. 397–408, 2012.

[17] M. R. Tucker, J. Olivier, A. Pagel, H. Bleuler, M. Bouri, O. Lambercy, J. del R Millán, R. Riener, H. Vallery, and R. Gassert, "Control strategies for active lower extremity prosthetics and orthotics: a review," *J. Neuroeng. Rehabil.*, vol. 12, no. 1, p. 1, 2015.

[18] D. Quintero, E. Reznick, D. J. Lambert, S. Rezazadeh, L. Gray, and R. D. Gregg, "Intuitive clinician control interface for a powered knee-ankle prosthesis: A case study," *IEEE J. Transl. Eng. Health Med.*, vol. 6, pp. 1–9, 2018.

[19] D. Quintero, D. Villarreal, D. Lambert, S. Kapp, and R. Gregg, "Continuous-phase control of a powered knee-ankle prosthesis: Amputee experiments across speeds and inclines," *IEEE Trans. Robot.*, vol. 34, no. 3, pp. 686–701, 2018.

[20] S. Yang and Q. Li, "Inertial sensor-based methods in walking speed estimation: A systematic review," *Sensors*, vol. 12, no. 5, pp. 6102–6116, 2012.

[21] A. Mannini and A. M. Sabatini, "Walking speed estimation using foot-mounted inertial sensors: Comparing machine learning and strap-down integration methods," *Medical engineering & physics*, vol. 36, no. 10, pp. 1312–1321, 2014.

[22] Q. Li, M. Young, V. Naing, and J. Donelan, "Walking speed estimation using a shank-mounted inertial measurement unit," *J. Biomech.*, vol. 43, no. 8, pp. 1640–1643, 2010.

[23] S. Yang, A. Laudanski, and Q. Li, "Inertial sensors in estimating walking speed and inclination: an evaluation of sensor error models," *Medical & biological engineering & computing*, vol. 50, no. 4, pp. 383–393, 2012.

[24] S. Beauregard and H. Haas, "Pedestrian dead reckoning: A basis for personal positioning," in *Proc. Workshop Position. Navig. Commun.*, 2006, pp. 27–35.

[25] Q. Fan, H. Zhang, Y. Sun, Y. Zhu, X. Zhuang, J. Jia, and P. Zhang, "An optimal enhanced kalman filter for a ZUPT-aided pedestrian positioning coupling model," *Sensors*, vol. 18, no. 5, p. 1404, 2018.

[26] R. Zhang, H. Yang, F. Höflinger, and L. M. Reindl, "Adaptive zero velocity update based on velocity classification for pedestrian tracking," *IEEE Sensors journal*, vol. 17, no. 7, pp. 2137–2145, 2017.

[27] Ö. Bebek, M. A. Suster, S. Rajgopal, M. J. Fu, X. Huang, M. C. Çavusoglu, D. J. Young, M. Mehregany, A. J. Van Den Bogert, and C. H. Mastrangelo, "Personal navigation via high-resolution gait-corrected inertial measurement units," *IEEE Trans Instrum Meas*, vol. 59, no. 11, pp. 3018–3027, 2010.

[28] A. M. Sabatini, C. Martelloni, S. Scapellato, and F. Cavallo, "Assessment of walking features from foot inertial sensing," *IEEE Trans. Biomed. Eng.*, vol. 52, no. 3, pp. 486–494, 2005.

[29] L. Ojeda and J. Borenstein, "Non-gps navigation for security personnel and first responders," *J. Navig.*, vol. 60, no. 3, pp. 391–407, 2007.

[30] B. Chen and Q. Wang, "Combining human volitional control with intrinsic controller on robotic prosthesis: A case study on adaptive slope walking," *Conf Proc IEEE Eng Med Biol Soc*, pp. 4777–4780, 2015.

[31] S. K. Park and Y. S. Suh, "Height compensation using ground inclination estimation in inertial sensor-based pedestrian navigation," *Sensors*, vol. 11, no. 8, pp. 8045–8059, 2011.

[32] W. Svensson and U. Holmberg, "An autonomous control system for a prosthetic foot ankle," in *4th IFAC Symposium on Mechatronic Systems*. IFAC, 2006, pp. 856–861.

[33] K. R. Embry, D. J. Villarreal, and R. D. Gregg, "A unified parameterization of human gait across ambulation modes," in *Conf Proc IEEE Eng Med Biol Soc*, 2016, pp. 2179–2183.

[34] K. R. Embry, D. J. Villarreal, R. L. Macaluso, and R. D. Gregg, "Modeling the kinematics of human locomotion over continuously varying speeds and inclines," *IEEE Trans. Neural Syst. Rehabil. Eng.*, vol. 26, no. 12, pp. 2342–2350, 2018.

[35] F. Horst, S. Lapuschkin, W. Samek, K.-R. Müller, and W. I. Schöllhorn, "Explaining the Unique Nature of Individual Gait Patterns with Deep Learning," *Sci. Rep.*, 2019.

[36] F. Horst, M. Mildner, and W. Schöllhorn, "One-year persistence of individual gait patterns identified in a follow-up study – A call for individualised diagnose and therapy," *Gait Posture*, vol. 58, 2017.

[37] M. J. Major and N. P. Fey, "Considering passive mechanical properties and patient user motor performance in lower limb prosthesis design optimization to enhance rehabilitation outcomes," *Phys. Ther. Rev.*, vol. 22, no. 4, 2017.

[38] E. Chehab, T. Andriacchi, and J. Favre, "Speed, age, sex, and body mass index provide a rigorous basis for comparing the kinematic and kinetic profiles of the lower extremity during walking," *J. Biomech.*, vol. 58, 2017.

[39] F. Moissenet, F. Leboeuf, and S. Armand, "Lower limb sagittal gait kinematics can be predicted based on walking speed, gender, age and BMI," *Sci. Rep.*, vol. 9, no. 1, 2019.

[40] K. Embry, D. Villarreal, R. Macaluso, and R. Gregg, "The effect of walking incline and speed on human leg kinematics, kinetics, and EMG," *IEEE DataPort*, 2018, http://dx.doi.org/10.21227/gk32-e868.

[41] T. Lenzi, L. Hargrove, and J. Sensinger, "Speed-adaptation mechanism: Robotic prostheses can actively regulate joint torque," *IEEE Robot Autom Mag*, vol. 21, no. 4, pp. 94–107, 2014.

[42] T. Flash and N. Hogan, "The coordination of arm movements: an experimentally confirmed mathematical model," *Journal of neuroscience*, vol. 5, no. 7, pp. 1688–1703, 1985.

[43] M. Grant and S. Boyd, "Graph implementations for nonsmooth convex programs," in *Recent Advances in Learning and Control*, ser. Lecture Notes in Control and Information Sciences. Springer-Verlag, 2008, pp. 95–110.

[44] D. J. Villarreal and R. D. Gregg, "A survey of phase variable candidates of human locomotion," in *Conf Proc IEEE Eng Med Biol Soc*, 2014, pp. 4017–4021.

[45] B. Griffin and J. Grizzle, "Nonholonomic virtual constraints for dynamic walking," in *Proc IEEE Conf Decis Control*, 2015, pp. 4053–4060.

[46] D. J. Villarreal, H. A. Poonawala, and R. D. Gregg, "A robust parameterization of human gait patterns across phase-shifting perturbations," *IEEE Trans. Neural Syst. Rehabil. Eng.*, vol. 25, no. 3, pp. 265–278, 2016.

[47] D. J. Villarreal and R. D. Gregg, "Controlling a powered transfemoral prosthetic leg using a unified phase variable," in *Wearable Robotics*. London, UK: Elsevier, 2020, ch. 24, pp. 487–505.

[48] R. Macaluso, K. Embry, D. Villarreal, and R. Gregg, "Parameterizing human locomotion across quasi-random treadmill perturbations and inclines," *IEEE Trans. Neural Syst. Rehabil. Eng.*, 2020, in review.

[49] K. Aminian, B. Najafi, C. Büla, P.-F. Leyvraz, and P. Robert, "Spatio-temporal parameters of gait measured by an ambulatory system using miniature gyroscopes," *J. Biomech.*, vol. 35, no. 5, pp. 689–699, 2002.

[50] LORD Sensing, "3DM-CX5-25 attitude and heading reference system," https://www.microstrain.com/sites/default/files/applications/files/3dm-cx5-25_datasheet_8400-0116rev_d.pdf, 2019.

[51] N. Abhayasinghe, I. Murray, and S. Sharif Bidabadi, "Validation of thigh angle estimation using inertial measurement unit data against optical motion capture systems," *Sensors*, vol. 19, no. 3, p. 596, 2019.

[52] B. T. West, K. B. Welch, and A. T. Galecki, *Linear mixed models: a practical guide using statistical software*. CRC Press, 2014.

[53] T. Pataky, "Generalized n-dimensional biomechanical field analysis using statistical parametric mapping," *J. Biomech.*, vol. 43, pp. 1976–82, 2010.

[54] B. Bechtold, "Violin plots for matlab," 2020. [Online]. Available: https://github.com/bastibe/Violinplot-Matlab

[55] A. M. Sabatini, C. Martelloni, S. Scapellato, and F. Cavallo, "Assessment of walking features from foot inertial sensing," *IEEE Trans. Biomed. Eng.*, vol. 52, no. 3, pp. 486–494, 2005.

[56] J. C. Alvarez, R. C. González, D. Alvarez, A. M. López, and J. Rodríguez-Uría, "Multisensor approach to walking distance estimation with foot inertial sensing," in *Conf Proc IEEE Eng Med Biol Soc*, 2007, pp. 5719–5722.

[57] Y. Song, S. Shin, S. Kim, D. Lee, and K. H. Lee, "Speed estimation from a tri-axial accelerometer using neural networks," in *Conf Proc IEEE Eng Med Biol Soc*, 2007, pp. 3224–3227.

[58] E. Reznick, K. R. Embry, and R. D. Gregg, "Predicting Individualized Joint Kinematics over a Continuous Range of Slopes and Speeds," in *IEEE Int Conf Biomed Robot Biomechatron*, 2020.